

Complex modular architecture around a simple toolkit of wing pattern genes

Steven M. Van Belleghem^{*1, 2}, Pasi Rastas^{*3}, Alexie Papanicolaou⁴, Simon H. Martin³, Carlos F. Arias^{2, 5}, Megan A. Supple², Joseph J. Hanly³, James Mallet⁶, James J. Lewis⁷, Heather M. Hines⁸, Mayte Ruiz¹, Camilo Salazar⁵, Mauricio Linares⁵, Gilson R. P. Moreira⁸, Chris D. Jiggins³, Brian A. Counterman⁺⁹, W. Owen McMillan^{+ 2} and Riccardo Papa⁺¹

¹. Department of Biology, Center for Applied Tropical Ecology and Conservation, University of Puerto Rico, Rio Piedras, Puerto Rico

². Smithsonian Tropical Research Institute, Apartado 0843-03092, Panamá, Panama

³. Department of Zoology, University of Cambridge, Cambridge CB2 3EJ, United Kingdom

⁴. Hawkesbury Institute for the Environment, Western Sydney University, Richmond, NSW 2753, Australia

⁵. Biology Program, Faculty of Natural Sciences and Mathematics, Universidad del Rosario, Carrera. 24 No. 63C-69, Bogota, D.C. 111221, Colombia.

⁶. Department of Organismic and Evolutionary Biology, Harvard University, Cambridge, MA, USA

⁷. Department of Ecology and Evolutionary Biology, Cornell University, 215 Tower Rd., Ithaca, NY 14853-7202

⁸. Department of Biology, Pennsylvania State University, University Park, Pennsylvania 16802, USA

⁹. PPG Biologia Animal, Departamento de Zoologia, Universidade Federal do Rio Grande do Sul, Av. Bento Gonçalves, 9500, Bloco IV, Prédio 43435, Porto Alegre, RS 91501-970, Brazil

¹⁰. Department of Biological Sciences, Mississippi State University, 295 Lee Boulevard, Mississippi State, MS 39762, USA

* Contributed equally

+ Contributed equally

Corresponding authors: vanbelleghemsteven@hotmail.com

1 **Abstract**

2 Identifying the genomic changes that control morphological variation and understanding how they generate
3 diversity is a major goal of evolutionary biology. In *Heliconius* butterflies, a small number of genes control
4 the development of diverse wing color patterns. Here, we used full genome sequencing of individuals across
5 the *Heliconius erato* radiation and closely related species to characterize genomic variation associated with
6 wing pattern diversity. We show that variation around color pattern genes is highly modular, with narrow
7 genomic intervals associated with specific differences in color and pattern. This modular architecture
8 explains the diversity of color patterns and provides a flexible mechanism for rapid morphological
9 diversification.

10 Recent adaptive radiations, such as the *Heliconius* butterflies¹, Galápagos finches² and African cichlids³,
11 offer insight into evolutionary and ecological forces that underlie diversification. Typically, ecological
12 opportunities allow natural and sexual selection to drive adaptive change and speciation. At a genetic level,
13 recruitment from ancient polymorphism, introgression of adaptive variants between populations and *de novo*
14 mutation are important sources of variation. However, the genetic architecture of the traits under natural and
15 sexual selection that facilitates rapid diversification remains largely unexplored.

16
17 In this study, we sequenced the genome of the Neotropical butterfly *Heliconius erato* and used re-sequenced
18 data from 116 additional individuals to dissect the architecture of genomic variation associated with their
19 vividly colored wing patterns. With over 400 different wing color forms among 46 described species⁴,
20 *Heliconius* represents one of the most visually diverse radiations in the animal kingdom and an excellent
21 system for establishing a broad and integrative view of morphological diversification. The evolution of scale
22 cells and the spatial coordinate system that controls wing pigmentation is a key innovation of the
23 Lepidoptera. Wing patterns are often under strong natural and sexual selection and these forces probably
24 shape much of the pattern diversity we see among the more than 160,000 butterfly and moth species⁵.

25
26 In *Heliconius*, conspicuous wing patterns are important for signaling toxicity to potential predators⁶ and
27 play a role in mate selection⁷. Natural selection favors Müllerian mimicry among toxic butterflies, resulting
28 in convergence between co-occurring species, as well as geographic divergence between populations of the
29 same species⁸. Among *Heliconius* butterflies, the genetic basis of this wing diversity has been studied for
30 nearly 60 years and more than 30 Mendelian loci have been described⁹. Over the past decade, however,
31 genetic research has shown that most of the complexity of color variation across *Heliconius* is actually
32 controlled by relatively few genes acting broadly across the fore- and hindwing¹⁰⁻¹⁶. These genes include
33 the transcription factor *optix*^{14,17}, the signaling ligand *wntA*¹⁵ and a cell cycle regulator *cortex*¹⁶. Hence, these
34 studies have revealed that a limited set of “toolkit”¹⁸ genes has been repeatedly used for both highly
35 divergent and convergent phenotypes in *Heliconius*, as well as other butterfly and moth species^{16,19,20}.
36 However, the key to wing pattern variation in *Heliconius* is not within the genes themselves, which are
37 strongly conserved at the amino acid level, but at nearby non-coding regions that control expression during
38 wing development¹⁴⁻¹⁶.

39
40 Here, we sequenced the genomes of 15 distinctly colored *H. erato* races and 8 closely related species to fully
41 describe the regulatory architecture driving adaptive evolution of the major genes acting in *Heliconius* wing
42 patterning (Figure 1). Our genomic survey included samples obtained near seven transition zones of
43 hybridizing *H. erato* races with divergent wing patterns (Figure 2A). In these hybrid zones, the high rate of

44 genetic admixture allows for detailed genotype by phenotype (G x P) association mapping to identify
45 discrete genomic intervals associated with color and pattern variation on *Heliconius* wings^{21,22}. We then
46 further investigated these intervals with a novel phylogenetic method for identifying conserved non-coding
47 regions in closely related non-hybridizing races and species. This combined strategy of association mapping
48 and phylogenetic inference resulted in a distinct set of narrow genomic intervals that corresponded to loci
49 described in early crossing experiments (Table S1 in SI section 1)⁹. All the intervals fell within non-coding
50 regions adjacent to color pattern genes that affect forewing band shape (*wntA*; Figure 3), red pigmentation
51 (*optix*; Figure 4) and a yellow hindwing bar (*cortex*; Figure 5). Our results underscore a highly modular
52 regulatory architecture that provides a flexible mechanism for rapid morphological change (Figure 6).

53 **Results and Discussion**

54 **Reference sequence and variants:** With more than 25 different wing pattern races, *H. erato* provides
55 exceptional opportunities to explore the links between genotype, phenotype, form and function. We first
56 constructed a high-quality reference genome by a combination of hybrid assembly coupled with high-
57 resolution linkage analysis. Our assembly and validation strategy generated one of the most contiguous and
58 accurate Lepidopteran genomes assembled thus far (SI section 2), which is available on the LepBase genome
59 browser. The final assembly consisted of 198 scaffolds with N50 length of over 10 Mb and a total assembly
60 length of 383 Mb. A total of 13,678 genes were identified using RNA-seq and a thorough annotation process
61 (SI section 3). To examine variation across our reference genome, we generated high (15-30x) coverage
62 whole-genome resequence data from 116 individuals of *H. erato* and closely related species. For the 101 *H.*
63 *erato* individuals sampled, we genotyped the majority of the non-repetitive portion of the genome (average
64 of 62% per individual, SI section 4.1). For the 15 individuals from the 8 outgroup species, the number of
65 positions that were genotyped for the outgroup species was lower, but above 40% for the most divergent
66 comparison (SI section 4.1).

67
68 **Genome-wide divergence across the *H. erato* color pattern radiation:** Within *H. erato*, individuals
69 clustered by geographic proximity rather than color pattern phenotype as has been previously reported²³
70 (Figure 1B and C). For example, forewing red banded *H. erato* races were found in all three
71 (Caribbean/Pacific Coast, East Amazonian, and West Amazonian) major geographic lineages (Figure 1).
72 Even within these broad geographic regions, individuals used in this study grouped together by sampling
73 location rather than wing morphology. Indeed, there was little genetic differentiation between *H. erato*
74 individuals sampled across major phenotypic transition zones, except around the genomic regions already
75 known to be involved in color pattern variation (Figure 2A). Genetic divergence as measured by F_{ST} was
76 close to zero across most of the genome, supporting the hypothesis of unhindered gene flow except at the
77 regions responsible for color pattern differences ($F_{ST} < 0.1$ in $97.07 \pm 0.03\%$ of 50 kb windows; SI section
78 3.3)²². This contrasted to three sharp peaks of genomic differentiation across known color pattern loci on
79 chromosome 10 near the *wntA* gene, on chromosome 15 near *cortex*, and on chromosome 18 near *optix* (red
80 in Figure 2B). As previously reported for the region around *optix*²², these regions showed the expected
81 signatures of selection, including reduced nucleotide diversity and elevated d_{XY} relative to genome-wide
82 averages (SI section 4.3).

83
84 **Associating genomic variation with color pattern diversity:** Genetic differences at the regions controlling
85 phenotypic variation in *Heliconius* are maintained by strong natural selection²⁴⁻²⁶. However, genotype by
86 phenotype (G x P) associations were often complex between any pairwise comparison reflecting different

87 histories of interactions between hybridizing taxa. Thus, at any specific comparison, associations often
88 spanned hundreds of thousands of base pairs around each color pattern locus (Figure 2B). Nonetheless, by
89 combining analysis of variation across multiple hybrid zones with phylogenetic analysis, we pinpointed
90 specific genomic intervals associated with specific aspects of phenotypic variation. This combination of G
91 x P association and phylogenetic analysis revealed a highly modular architecture to the variation around
92 major color pattern loci.

93
94 **Modular architecture of forewing black color variation:** Recent genetic mapping coupled with studies of
95 gene expression, suggest that a single gene, *wntA*, is driving much of the forewing pattern variation across
96 *Heliconius* species²⁷. Indeed, our G x P association highlighted a 100 kb non-coding region near *wntA* on
97 chromosome 10 (Figure 3). Clusters of fixed SNPs defined discrete genomic intervals associated with the
98 phenotypic effects of the *Sd*, *St* and *Ly* loci that were first described by Sheppard and colleagues more than
99 30 years ago⁹. Variation at *Sd*, *St*, and *Ly* was predicted to control patterning across the middle to the most
100 distal sections of the forewing respectively (Figure 3A). Consistent with this hypothesis, we identified: 1) a
101 25 kb region of fixed differences between *H. e. notabilis* and *H. e. lativitta* that differed across the lower
102 (*Sd*) and the middle (*St*) region of the forewing (purple in Figure 3B), 2) a narrow peak of association
103 between *H. e. notabilis* and *H. e. etylus* that differed only in the lower forewing region (*Sd*) (blue in Figure
104 3B), and 3) a broad region of association that spans roughly 60 kb and appears to be composed of several
105 distinct peaks between *H. e. erato* and *H. e. hydara* from French Guiana that differed in *St* and *Ly* (orange
106 in Figure 3B). Comparisons between races with identical forewings showed no G x P association across any
107 of these regions (green in Figure 3B).

108
109 To further refine the regions associated with forewing band pattern, we used a novel tree weighting approach
110 called *Twisst* (Topology weighting by iterative sampling of subtrees; see methods)²⁸, to explore how
111 phylogenetic relationships varied around *wntA*. We hypothesize that the genomic variation underlying wing
112 pattern differences should cluster individuals by wing pattern rather than geographic proximity. Sliding
113 window phylogenetic comparisons identified four narrow genomic intervals near *wntA* that were strongly
114 associated with changes in the spatial distribution of black scales on the forewing (Figure 3C). The first
115 region was a 10 kb interval roughly 50 kb upstream of *wntA* (blue in Figure 3C) that supported the
116 monophyletic grouping of races that are partially black in the lower midsection of the forewing extending
117 just distal of the discal cell region. Similarly, a separate 8 kb interval roughly 35 kb upstream of *wntA*
118 grouped geographically distant individuals with similar distribution of black scales across most of the distal
119 mid-section of the forewing (*St* interval) (green in Figure 3C). Finally, two additional regions, one 25 kb
120 upstream of *wntA* and another centered on *wntA*, grouped all individuals that were partially black in the

121 upper section of the forewing (*Ly* intervals) (orange in Figure 3C). Although, the region centered on *wntA*
122 showed some support for tree topologies based on geographic proximity, we still considered it a possible
123 color pattern interval because the phenotypic grouping is more strongly supported than geographic grouping.
124 Other areas across this region supporting the phenotypic tree also showed similar support for tree topologies
125 based on geographic proximity and were not considered as candidate color pattern intervals.

126
127 Our genomic analysis also confirmed a new locus (*Ro*) responsible for pattern variation in the most distal
128 region of the forewing band²⁹. Comparisons of *H. e. notabilis* and *H. e. lativitta* showed an approximately
129 71 kb region associated with pattern differences in the upper forewing (purple in Figure 3B). Similar to the
130 *wntA* region, G x P associations were localized to non-genic regions near two genes, the *Heliconius* homolog
131 of *ventral veins lacking* gene (*vvl*) and the homolog of *radial spoke head protein 3* (*rsp3*). The transcription
132 factor *vvl* is involved in the formation of specific wing veins, neuronal differentiation and steroid production
133 in *Drosophila*^{30–32}. The *rsp3* gene encodes a kinase A-anchoring protein that scaffolds the cAMP-dependent
134 protein kinase holoenzyme (PKA) and is involved in numerous regulatory events in the cell³³. The absence
135 of geographically independent hybrid zones for this phenotype limited our ability to further resolve this
136 region with phylogenetic weighting. Although spatial expression patterns of *wntA* in *Heliconius* have been
137 shown to prefigure variation in this upper region of the forewing¹⁵, it is likely that one or both of these genes
138 interact with *wntA* to shape this variation. Such epistatic interactions are commonly observed in color pattern
139 variation in *Heliconius*^{34–36}.

140
141 **Modular architecture of red pattern variation:** Regulation of red patterns across the fore- and hindwing of
142 *H. erato*, known to be under control of the gene *optix*^{14,17}, was also highly modular. We identified discrete
143 genomic intervals near *optix* that were associated with the presence of red hindwing rays, a red patch
144 ("dennis") in the proximal part of the forewing and a red forewing band. We use the original nomenclature
145 in *H. erato* for these different pattern elements: *R* for red hindwing "rays", *D* for a red "dennis" forewing
146 patch and *Y* for forewing "band" color (Figure 4A)⁹.

147
148 Associations between individuals that differed across all three pattern elements, the so-called "dennis-rayed"
149 and "postman" phenotypes, were strongly clustered in a 69 kb region downstream of *optix* (Figure 4B)²⁶.
150 Within this 69 kb region, G x P associations between hybridizing *H. e. amalfreda* and *H. e. erato*, which
151 differ only in absence/presence of hindwing rays, were clustered in a 7 kb interval (Figure 4B). In this
152 interval, *H. e. amalfreda* possessed the postman haplotype, which contrasts with the rest of the 69 kb region
153 where *H. e. amalfreda* shared a haplotype with *H. e. erato*. Phylogenetic trees constructed from this region,
154 grouped *H. e. amalfreda* with postman phenotypes that lack rays (red shading in Figure 4C). Unexpectedly,

155 the tree across this interval clustered the outgroup species, *H. telesiphe*, *H. hortense*, *H. hecalesia*, *H.*
156 *clysonymus*, and *H. sara* on a derived node with all rayed *H. erato* races (SI section 5.3.2). *Heliconius*
157 *hecalesia*, *H. hortense*, and *H. clysonymus* all have large red hindwing patches, whereas, *H. sara* and *H.*
158 *telesiphe* possess much smaller red spots on the underside of their hindwing. This pattern contrasts with the
159 phylogenetic placement of these species in the tree constructed with data from the rest of the genome (Figure
160 1A), possibly reflecting historical introgression of modular elements among species closely related to *H.*
161 *erato*. Such patterns of introgression have also been observed in other closely related *Heliconius* species¹³⁷.
162

163 Genomic intervals strongly associated with forewing band color (*Y*) and the red dennis patch (*D*) could be
164 similarly localized using the combination of G x P association and phylogenetic weighting. For forewing
165 band color, we identified two distinct and narrow intervals separated by approximately 20 kb (yellow in
166 Figure 4B and C). In these regions, there were 15 fixed SNPs that distinguished butterflies with a red
167 forewing band from those that lacked red. Phylogenetic trees from this region strongly supported clustering
168 of the red banded phenotypes *H. telesiphe*, *H. hermathena*, *H. e. favorinus* and *H. e. hydara*, whereas *H.*
169 *himera*, *H. hortense*, *H. clysonymus* and *H. hecalesia*, all of which lack red on the forewing, grouped with
170 the yellow banded *H. erato* races (Figure 4C and SI section 5.3.2). Finally, we identified several intervals
171 associated with the red dennis patch. For this analysis, we focused primarily on genetic variation within *H.*
172 *himera*. *Heliconius himera* has red on the hindwing similar to rays, but lacks the dennis patch. Therefore,
173 comparing *H. himera* and *H. erato* races with a dennis/rays phenotype allowed us to separate the dennis
174 from the rays elements. Across the 69 kb region, there was a 12 kb area where *H. himera* genotypes were
175 similar to the postman haplotype (grey in Figure 4B). Phylogenetic weighting analysis in this area strongly
176 supported the grouping of *H. himera* individuals by color pattern phenotype with postman races from both
177 sides of the Amazon basin (grey in Figure 4C).
178

179 ***Independent modules generate convergent yellow hindwing bar phenotypes:*** Recent association and
180 expression data implicated the gene *cortex* as an important gene controlling a variety of pattern elements
181 across the *Heliconius* wing, including presence or absence of yellow hindwing bar in *H. erato*, known as
182 the *Cr* locus^{9,16}. In *H. erato*, we identified two discrete regions containing clusters of fixed sites associated
183 with a yellow hindwing bar in two geographically isolated, yet phenotypically similar, *H. erato* races (Figure
184 5). The Peruvian races *H. e. favorinus* and *H. e. emma* differed across an interval consisting of 269 fixed
185 SNPs over 100 kb roughly centered on *cortex* (red in Figure 5). Eight of these SNPs fell within the coding
186 region of *cortex*, but only one resulted in amino acid substitution (an arginine to lysine at scaffold
187 Herato1505 position 2,087,610). Curiously, a different region distinguished the Panamanian races, *H. e.*
188 *demophon* and *H. e. hydara* (green in Figure 5), which show a similar difference in the presence/absence of

189 a yellow hindwing bar. In this hybrid zone, there was a cluster of fixed differences located roughly 100 kb
190 away and centered on the *Heliconius* homolog of *parn*, a poly(A)-specific ribonuclease. These association
191 differences are consistent with the independent evolution of the yellow hindwing bar on either side of the
192 Andes^{34,38}.

193
194 In *H. erato*, there are other color pattern elements controlled by variation at this locus, including the
195 presence/absence of white hindwing fringes and yellow forewing line³⁹, but our sampling of *H. erato* races
196 did not allow us to distinguish these elements (SI section 5.4). The hybrid zone comparisons *H. e. notabilis*/
197 *H. e. lativitta* and *H. e. notabilis*/*H. e. etylus* also showed increased F_{ST} estimates near the *cortex* gene, but
198 no pattern of perfect association was observed for these comparisons. Crossing experiments have suggested
199 possible epistatic interactions between *cortex* and *wntA*^{38,40}, which provides a possible explanation for this
200 increased divergence without any phenotypic effect known to be directly controlled by the *cortex* locus.
201 Furthermore, the phenotypic effects of alleles at this locus can be dramatic in other *Heliconius* species¹⁶,
202 suggesting that this locus interacts broadly with the other *Heliconius* patterning loci^{10,41}.

203
204 **Modular regulatory architecture and pattern diversity within *H. erato*:** Less than 0.2% of the genome was
205 associated with wing pattern diversity across the *H. erato* radiation. This variation was highly modular and
206 fell in non-coding regions near color patterning genes, including *optix*, *wntA* and *cortex*¹⁴⁻¹⁶ and a less well-
207 documented color pattern locus (*Ro*) that controls spatial variation of melanin in the upper forewing. Based
208 on the proximity of these mostly non-coding intervals to known patterning genes, it is likely they represent
209 *cis*-regulatory regions modulating the spatial expression of key patterning genes in discrete areas of the
210 developing wing. In *Heliconius*, this modularity of *cis*-regulatory architecture provides a readily adopted
211 mechanism for rapid evolution of novel morphologies.

212
213 Both shuffling of existing modules and *de novo* evolution of new modules is associated with phenotypic
214 diversity in *H. erato*. Indeed, we can recreate the color pattern diversity across the *H. erato* radiation using
215 a combination of ten non-genic regions, near four color pattern genes (Figure 6). This conclusion is perhaps
216 best exemplified in the distribution of genetic variation around *wntA*, where different color pattern races
217 have different combinations of four distinct genomic intervals. These different intervals likely regulate the
218 expression of *wntA* in different areas of the forewing to adjust the position, size, and shape of the forewing
219 to closely match patterns in other co-occurring warningly colored butterfly species. Within this modular
220 framework, recombination can reshuffle existing regulatory variation to generate new combinations of
221 regulatory elements and new wing pattern phenotypes. Recombination of color pattern modules and
222 introgression into other populations is likely driven by high rates of gene flow between adjacent populations.

223 For example, *H. e. amalfreda* appears to have evolved via recombination of regulatory variation between
224 rayed (*H. e. erato*) and red-banded (*H. e. hydara*) haplotypes that instantaneously generated a novel wing
225 pattern, a process which closely mirrors the one recently described in the co-mimetic forms of *H.*
226 *melpomene*³⁷.

227
228 New regulatory modules associated with wing pattern variation can also evolve *de novo*, further increasing
229 the flexibility of these regions to generate pattern diversity. This was evident in the independent evolution
230 on the yellow hindwing bar in the *H. erato* clade (Figure 5), but also in the comparison of regulatory
231 variation around the red patterning locus between *H. erato* and its co-mimic *H. melpomene*. Red pattern
232 variation in the two species is similarly generated by regulatory differences at the *optix* locus¹⁴, and the
233 genomic position and order of its *cis*-regulatory elements is broadly similar²⁶. Furthermore, in both species
234 distinct intervals were associated with different red pattern elements and ‘enhancer shuffling’ through
235 recombination has similarly generated novel red pattern phenotypes³⁷. This implies considerable
236 conservation of function of *optix cis*-regulatory regions that were re-used to generate the convergent patterns
237 that underlie mimicry. Nonetheless, the precise elements associated with placement of red in discrete areas
238 of the fore- and hindwing are not homologous in the two species (SI, section 5.3.3). Thus, convergent
239 patterns are clearly independently derived in the two radiations by the parallel evolution of new enhancer
240 variation.

241

242 **Conclusions**

243 Our results reconcile decades of genetic and genomic studies of *Heliconius* color pattern variation^{9,42}. For
244 the first time, we were able to place an entire radiation within a single genomic framework. We reinforce
245 the role of a simple toolkit of a few color pattern genes and demonstrate that pattern diversity is likely
246 generated by the regulatory complexity around these genes. We characterized a discrete number of 1-7 kb
247 intervals that modulate phenotypic variation, and show that divergent and convergent morphologies, are the
248 product of enhancer shuffling and *de novo* independent evolution of these modules. Overall, our work
249 provides a genomic framework to further explore this regulatory complexity. The regions we identified may
250 contain a number of distinct regulatory elements that may be further resolved with chromatin accessibility
251 data⁴³ and studied in detail with targeted genome editing. Such an integrated genomic view promises to
252 accelerate our understanding of the links between genotype and phenotype and how they play out on a
253 developing butterfly wing. This research has broader ramifications because the small number of genes
254 shown to generate wing pattern variation across *Heliconius* have been implicated in pattern variation in
255 other butterflies and moths^{16,19,44}. Thus, the *Heliconius* wing pattern loci appear to be ‘genomic hotspots’
256 that underlie the evolution of phenotypic diversity in Lepidoptera. The radiation of warning colors in *H.*

257 *erato* provides an example of regulatory complexity generated by a small toolkit of genes. This may well be
258 a common hallmark of rapid morphological diversification in adaptive radiations.

259

260 **Data accessibility**

261 Sequencing data was submitted to the Sequence Read Archive (SRA) with BioProject accession
262 PRJNA324415; Genome assembly data: SAMN05578372-SAMN05578377, RNAseq data: SRR616674-
263 SRR616691, SAMN05578182-SAMN05578206, Linkage map data: SAMN05572290-SAMN05572390
264 and re-sequencing data: SAMN05224096- SAMN05224211.

265

266 **Author contributions**

267 S.M.V.B., B.A.C., W.O.M. and R.P. designed the study and wrote the paper. P.R., A.P. and J.J.M conducted
268 genome assembly. P.R. conducted linkage map and genome quality assessment. A.P. conducted genome
269 annotation. S.M.V.B. conducted population genomic, phylogenetic and comparative genomic analyses.
270 M.R., M.A.S., H.H. and J.J.H. conducted comparative genomic analyses. S.H.M. contributed scripts for
271 *Twisst* analyses. B.A.C., W.O.M., R.P., H.H., C.D.J., J.M., M.L., C.S., C.F.A. and G.M. collected samples
272 for sequencing.

273

274 **Acknowledgments**

275 We thank Adriana Tapia for maintaining the *H. erato* genome line and for generating our mapping family
276 and Marta Vargas and Claudia Rosales for Illumina library preparation. We acknowledge the University of
277 Puerto Rico, the Puerto Rico INBRE grant P20 GM103475 from the National Institute for General Medical
278 Sciences (NIGMS), a component of the National Institutes of Health (NIH); CNRS Nouraugues and CEBA
279 awards (BAC); National Science Foundation awards DEB-1257839 (BAC), DEB-1257689 (WOM), DEB-
280 1027019 (WOM); awards 1010094 and 1002410 from the Experimental Program to Stimulate Competitive
281 Research (EPSCoR) program of the National Science Foundation (NSF) for computational resources; and
282 the Smithsonian Institution. This research was supported in part by Lilly Endowment, Inc., through its
283 support for the Indiana University Pervasive Technology Institute, and in part by the Indiana METACyt
284 Initiative. The Indiana METACyt Initiative at IU is also supported in part by Lilly Endowment, Inc.

285

286 **References**

- 287 1. Dasmahapatra, K. K. *et al.* Butterfly genome reveals promiscuous exchange of mimicry
288 adaptations among species. *Nature* **487**, 94–98 (2012).
- 289 2. Lamichhane, S. *et al.* Evolution of Darwin's finches and their beaks revealed by genome
290 sequencing. *Nature* **518**, 371–375 (2015).
- 291 3. Brawand, D. *et al.* The genomic substrate for adaptive radiation in African cichlid fish.

- 292 *Nature* **513**, 375–381 (2014).
- 293 4. Lamas, G. in *Hesperioidea – Papilionoidea*. Gainesville, Florida: Association for Tropical
294 *Lepidoptera*. (ed. Lamas, G.) 261–274 (Scientific Publisher, 2004).
- 295 5. Nijhout, H. F. *The development and evolution of butterfly wing patterns*. (Smithsonian
296 Institution Press, 1991).
- 297 6. Chouteau, M., Arias, M. & Joron, M. Warning signals are under positive frequency-
298 dependent selection in nature. *Proc. Natl. Acad. Sci.* **113**, 2164–2169 (2016).
- 299 7. Naisbit, R. E., Jiggins, C. D. & Mallet, J. Disruptive sexual selection against hybrids
300 contributes to speciation between *Heliconius cydno* and *Heliconius melpomene*. *Proc. Biol.*
301 *Sci.* **268**, 1849–1854 (2001).
- 302 8. Turner, J. R. G. A tale of two butterflies. *Nat. Hist.* **84**, 28–37 (1975).
- 303 9. Sheppard, P. M., Turner, J. R. G., Brown, K. S., Benson, W. W. & Singer, M. C. Genetics
304 and the evolution of Mullerian mimicry in *Heliconius* Butterflies. *Philos. Trans. R. Soc. B*
305 *Biol. Sci.* **308**, 433–610 (1985).
- 306 10. Joron, M. *et al.* A conserved supergene locus controls colour pattern diversity in
307 *Heliconius* butterflies. *PLoS Biol.* **4**, e303 (2006).
- 308 11. Papa, R. *et al.* Multi-allelic major effect genes interact with minor effect QTLs to control
309 adaptive color pattern variation in *Heliconius erato*. *PLoS One* **8**, e57033 (2013).
- 310 12. Kronforst, M. R., Kapan, D. D. & Gilbert, L. E. Parallel genetic architecture of parallel
311 adaptive radiations in mimetic *Heliconius* butterflies. *Genetics* **174**, 535–539 (2006).
- 312 13. Kapan, D. D. *et al.* Localization of müllerian mimicry genes on a dense linkage map of
313 *Heliconius erato*. *Genetics* **173**, 735–757 (2006).
- 314 14. Reed, R. D. *et al.* *optix* drives the repeated convergent evolution of butterfly wing pattern
315 mimicry. *Science* **333**, 1137–1141 (2011).
- 316 15. Martin, A. *et al.* Diversification of complex butterfly wing patterns by repeated regulatory
317 evolution of a Wnt ligand. *Proceedings of the National Academy of Sciences* **109**, 12632–
318 12637 (2012).
- 319 16. Nadeau, N. *et al.* The gene *cortex* controls mimicry and crypsis in butterflies and moths.
320 *Nature* **534**, 106–110 (2016).
- 321 17. Martin, A. *et al.* Multiple recent co-options of *Optix* associated with novel traits in
322 adaptive butterfly wing radiations. *Evodevo* **5**, 7 (2014).
- 323 18. Carroll, S. B. Evo-Devo and an expanding evolutionary synthesis: a genetic theory of
324 morphological evolution. *Cell* **134**, 25–36 (2008).
- 325 19. Gallant, J. R. *et al.* Ancient homology underlies adaptive mimetic diversity across
326 butterflies. *Nat. Commun.* **5**, 1–10 (2014).
- 327 20. Van't Hof, A. E. The industrial melanism mutation in British peppered moths is a
328 transposable element. *Nature* **534**, 102–105 (2016).
- 329 21. Rosser, N., Dasmahapatra, K. K. & Mallet, J. Stable *Heliconius* butterfly hybrid zones are
330 correlated with a local rainfall peak at the edge of the Amazon basin. *Evolution* **68**, 3470–
331 3484 (2014).
- 332 22. Supple, M., Papa, R., Hines, H. M., McMillan, W. O. & Counterman, B. A. Divergence
333 with gene flow across a speciation continuum of *Heliconius* butterflies. *BMC Evol. Biol.*
334 **15**, 204 (2015).
- 335 23. Hines, H. M. *et al.* Wing patterning gene redefines the mimetic history of *Heliconius*
336 butterflies. *Proc. Natl. Acad. Sci. U. S. A.* **108**, 19666–19671 (2011).
- 337 24. Mallet, J. & Barton, N. H. Strong natural selection in a warning-color hybrid zone.
338 *Evolution* **43**, 421–431 (1989).

- 339 25. Kapan, D. D. Three-butterfly system provides a field test of müllerian mimicry. *Nature*
340 **409**, 18–20 (2001).
- 341 26. Supple, M. a *et al.* Genomic architecture of adaptive color pattern divergence and
342 convergence in *Heliconius* butterflies. *Genome Res.* **23**, 1248–57 (2013).
- 343 27. Martin, A. *et al.* Diversification of complex butterfly wing patterns by repeated regulatory
344 evolution of a Wnt ligand. *Proc. Natl. Acad. Sci. U. S. A.* **109**, 12632–12637 (2012).
- 345 28. Martin, S. H. & Van Belleghem, S. M. Exploring evolutionary relationships across the
346 genome using topology weighting. *BioRxiv* (2016).
- 347 29. Nadeau, N. J. *et al.* Population genomics of parallel hybrid zones in the mimetic
348 butterflies, *H. melpomene* and *H. erato*. *Genome Res.* **24**, 1316–1333 (2014).
- 349 30. Danielsen, E. T. *et al.* Transcriptional control of steroid biosynthesis genes in the
350 *Drosophila* prothoracic gland by Ventral veins lacking and Knirps. *PLoS Genet.* **10**,
351 e1004343 (2014).
- 352 31. de Celis, J. F., Llimargas, M. & Casanova, J. *ventral veinless*, the gene encoding the Cfla
353 transcription factor, links positional information and cell differentiation during embryonic
354 and imaginal development in *Drosophila melanogaster*. *Development* **121**, 3405–3416
355 (1995).
- 356 32. Meier, S., Sprecher, S. G., Reichert, H. & Hirth, F. *ventral veins lacking* is required for
357 specification of the tritocerebrum in embryonic brain development of *Drosophila*. *Mech.*
358 *Dev.* **123**, 76–83 (2006).
- 359 33. Jivan, a., Earnest, S., Juang, Y.-C. & Cobb, M. H. Radial spoke protein 3 is a mammalian
360 protein kinase A-anchoring protein that binds ERK1/2. *J. Biol. Chem.* **284**, 29437–29445
361 (2009).
- 362 34. Jiggins, C. D. & Mcmillan, W. O. The genetic basis of an adaptive radiation: warning
363 colour in two *Heliconius* species. *Proc. R. Soc. B* **264**, 1167–1175 (1997).
- 364 35. Baxter, S. W., Johnston, S. E. & Jiggins, C. D. Butterfly speciation and the distribution of
365 gene effect sizes fixed during adaptation. *Heredity (Edinb)*. **102**, 57–65 (2009).
- 366 36. Huber, B. *et al.* Conservatism and novelty in the genetic architecture of adaptation in
367 *Heliconius* butterflies. *Heredity (Edinb)*. **114**, 515–524 (2015).
- 368 37. Wallbank, R. W. R. *et al.* Evolutionary novelty in a butterfly wing pattern through
369 enhancer shuffling. *PLoS Biol.* **14**, e1002353 (2016).
- 370 38. Maroja, L. S., Alschuler, R., Mcmillan, W. O. & Jiggins, C. D. Partial complementarity of
371 the mimetic yellow bar phenotype in *Heliconius* butterflies. *PLoS One* **7**, e48627 (2012).
- 372 39. Sheppard, P. M., Turner, J. R. G., Brown, K. S., Benson, W. W. & Singer, M. C. Genetics
373 and the evolution of Müllerian mimicry in *Heliconius* butterflies. *Philos. Trans. R. Soc. B*
374 *Biol. Sci.* **308**, 433–610 (1985).
- 375 40. Mallet, J. The genetics of warning colour in Peruvian hybrid zones of *Heliconius erato* and
376 *H. melpomene*. *Proc. R. Soc. B* **236**, 163–185 (1989).
- 377 41. Joron, M. *et al.* Chromosomal rearrangements maintain a polymorphic supergene
378 controlling butterfly mimicry. *Nature* **477**, 203–206 (2011).
- 379 42. Kronforst, M. R. & Papa, R. The functional basis of wing patterning in *Heliconius*
380 butterflies: The molecules behind mimicry. *Genetics* **200**, 1–19 (2015).
- 381 43. Lewis, J. J. *et al.* ChIP-Seq-annotated *Heliconius erato* genome highlights patterns of cis-
382 regulatory evolution in Lepidoptera. *CellReports* **16**, 2855–2863 (2016).
- 383 44. Martin, A. & Reed, R. D. Wnt signaling underlies evolution and development of the
384 butterfly wing pattern symmetry systems. *Dev. Biol.* (2014).
- 385

386 **Methods**

387 **Scaffold assembly and validation:** The *H. erato* (race *demophoon*) genome was assembled using Illumina
388 paired-end reads with different insert sizes and partially gap filled with PacBio data (Table S2 in SI section
389 2.1). Illumina data was produced according to the ALLPATHS-LG assembly protocol⁴⁵ with the paired-end
390 library originating from a single individual and the mate pair libraries from a second, sibling, individual. An
391 initial assembly was performed with ALLPATHS-LG using default parameters and the reads were mapped
392 back to the assembly to acquire accurate distributions of fragment size for each library. Next, contaminant
393 small fragment sequences were purged from the paired-end and mate-pair libraries. Reads were error-
394 corrected using the software Blue⁴⁶. A *kmer* database was built from the raw paired-end data and used to
395 remove unsupported reads from mate-paired libraries. This step reduced polymorphism that may cause
396 erroneous assembly. The PacBio data were error-corrected using the Illumina data and the LoRDEC
397 software⁴⁷.

398 Five assemblies were obtained using different combinations of raw or error-corrected Illumina data. Each
399 assembly was quality checked against approximately 4 Mb of BAC sequences using nucmer⁴⁸. All
400 assemblies gave similar amounts of gapped sequence (about 10% of the base pairs), which reflects long
401 simple repeats scattered across the genome. The assembly with the best statistics (i.e. highest N50's and
402 best alignment to BAC) was then post-processed to replace putative tandem repeats with Ns. Small repetitive
403 scaffolds and putative redundant haplotype sequences were removed and based on a combination of “all-
404 versus-all” alignments and depth of coverage estimates prior to performing ALLPATHS-LG scaffolding.
405 Gaps were then filled using the filled fragment pairs, the corrected PacBio data and the small scaffolds that
406 had been previously removed using PBJelly⁴⁹. PBJelly was run three times iteratively to balance sensitivity
407 and specificity and the final assembly, called Hera_Stage1, had a length of 402.8 Mb and scaffold N50 of
408 612 kb, respectively. The assembly process with associated statistics are provided in Table S2 and Figure
409 S1 in SI section 2.2.

410
411 **Linkage mapping:** We generate a high-resolution linkage map by sequencing a backcross family generated
412 from our focal genomic line (Figure S2 in SI section 2.3). Our strategy was to identify markers by coupling
413 high-coverage, whole-genome sequencing (30-40x) of each parent with low coverage (5x-10x) sequencing
414 of their offspring. The low sequencing coverage of the offspring makes it difficult to determine individual
415 genotypes with high accuracy. We therefore developed an in-house pipeline utilizing the mpileup command
416 in SAMtools⁵⁰ to produce genotype posteriors over a candidate set of 6.7 million SNPs. These genotype
417 posteriors were used to construct a linkage map with Lep-Map3 (sourceforge.net/projects/lep-map3/) a new
418 linkage mapping software developed from the Lep-Map1/2 software^{51,52}.

419 The linkage map was constructed with Lep-Map3 as follows (see Figure S3 in SI section 2.3): First, to obtain

420 the most accurate parent genotypes, we calculated the parental genotype posteriors using the combined
421 information from parents and offspring using the ParentCall module (Lep-Map2). Next, we calculated pair-
422 wise LOD scores between markers with zero recombination rate ($\theta=0$) using the module
423 SeparateIdenticals (Lep-Map3) with $\text{lodLimit}=26.5$, $\text{informativeMask}=12$ and $\text{numParts}=20$. This step
424 identified markers that segregated identically. The 20 most abundant identical maternal markers were used
425 as the chromosome prints (each maternal marker in a chromosome segregates identically as there is no
426 recombination in the female in *Heliconius* butterflies). In this step, we could identify 20 of the 21
427 chromosomes, because we found that chromosome 2 was completely homozygous in the mother. To identify
428 chromosomes, especially chromosome 2, in the paternal linkage map, identical paternal markers were joined
429 using module JoinLGs (Lep-Map3) with recombination rate $\theta=0.01$ and LOD score limit $\text{lodLimit}=20$.
430 More precisely, the linkage groups could be linked together for chromosome 2 by inspecting the markers at
431 nearby positions in the assembly. These paternal markers clustered to 21 linkage groups identifying
432 chromosome 2 and the same 20 chromosomes that were found in the maternal map. Next, the module
433 ShortPath (Lep-Map3) was run on the identical paternal markers. This module finds the longest shortest
434 path in a marker graph (i.e. the longest path in graph for which the shortest path is chosen between pairs of
435 markers), where markers are nodes and each marker pair have been connected with an edge of length $4n -$
436 3 , if there are n detected recombinations (different genotypes considering both phases in this case) between
437 the markers. The best paths were manually checked to determine the final order of the markers. After the
438 maternal and paternal markers were placed within a linkage framework (Table S3 in SI section 2.3), we
439 added the remaining markers into this framework using JoinIdenticals (Lep-Map3), with LOD score limits
440 of 25 and 20, for paternal and maternal markers, respectively. The 1.2 million markers that were
441 heterozygous in both parents were discarded ($\text{informativeMask}=12$). Finally, the identified linkage groups
442 (chromosomes) were named to reflect the nomenclature of the *H. melpomene* genome. We were able to
443 easily identify homologous chromosomes by mapping the flanking regions of each marker to the *H.*
444 *melpomene* genome¹. Our final linkage map covered all 21 chromosomes, including the Z chromosome.

445
446 **Assembly correction and chromosomal scaffolding:** We used our high-resolution linkage map to error
447 correct and improve our genome assembly. To do this, we first manually identified scaffolds that were
448 inconsistent with our linkage map. About 10% of the scaffolds, representing 62 Mb, had such errors. Due
449 to the high-density of markers on our linkage map, most errors were localized within a few kb. These errors
450 generally fell at a gap sequence meaning that the scaffolding step of the assembly process, rather than the
451 creation of contigs, caused most misassemblies. The scaffolds in the assembly with errors were cut to produce
452 an error-free assembly. The assembly was also separated into chromosomes at this point. There was about
453 16 Mb of gapped sequence in the Herato_stage1 assembly. The 34 scaffolds that failed to map to

454 chromosomes totaled 3.7 Mb, 3.5 Mb of which were bacterial genome sequence and the rest was mainly
455 very highly repetitive haplotypes that failed to create substantially long (> 3 kb) contigs.
456 We produced the final assembly by integrating information from two independent *de novo* assemblies to
457 gap fill our oriented stage2 assembly. The first was an ALLPATHS-LG assembly generated from the same
458 Illumina paired-end and mate-paired dataset, and assembled as follows. Illumina paired-end and
459 mate-pair data were subsampled to prescribed coverage depth according to Gnerre et al. 2011⁴⁵ and
460 assembled using ALLPATHS-LG with “HAPLOIDIFY = TRUE” and “CLOSE_UNIPATH_GAPS =
461 False”. The resulting assembly was improved by performing 3 iterations of PBJelly⁴⁹, incorporating prior
462 PBJelly assemblies into subsequent iterations. The second was an assembly of an additional sibling female
463 individual using approximately 100x coverage of 2 x 250 Illumina data generated from PCR free libraries.
464 The genome of this individual was assembled using DISCOVAR *de novo*^{53,54}. The scaffolds that spanned
465 gaps in our assembly were extracted from the BWA-MEM⁵⁵ produced bam files using in-house software.
466 This software used a variant of Smith-Waterman local alignment⁵⁶ to compute the best alignment to fix gaps.
467 Both positive and negative gaps were considered. The alignment parameters used were +1 for nucleotide
468 match, -4 for mismatch, -8 for gap open and -1 for gap extension. Gaps were filled iteratively, using the
469 independent ALLPATHS assembly first. Here we required an alignment score of 100 across a 4 kb region
470 on each side of a gap for the gap to be filled. Regions with multiple gaps were joined as if they contained a
471 single large gap. Finally, we filled remaining gaps using the DISCOVAR assembly. In this case, we used
472 alignment to 2 kb regions around each gap. Using this strategy, we reduced the number of gaps in our
473 assembly to 5.2 Mb. Assembly completeness, as assessed against a benchmarked set of 2,675 single-copy
474 orthologues using BUSCO⁵⁷ was 82% (2,179) in the *H. erato* genome and a further 11% were present, but
475 marked as ‘fragmented’. These BUSCO results were similar to those for other high quality lepidopteran
476 genomes (Table S8 in SI section 2.4). We assembled 5 of 20 autosomes and the Z chromosome into single
477 scaffolds. We failed to identify a W chromosome, likely because of its highly repetitive nature. See Figure
478 S4 in the SI section 2.3 for the completeness of the scaffolding in the final *H. erato* genome assembly.

479
480 **Genome Annotation:** Annotation of the genome was performed using Just_Annotate_My_Genome (JAMg;
481 <https://github.com/genomecuration/JAMg>). To facilitate annotation, we used RNASeq data generated from
482 different life stages and tissue types (Table S9 in SI section 3). These data include recent Illumina 2x250
483 data, 454 data, and archival Illumina 2x50 data. All data were preprocessed using “justpreprocessmyreads”
484 (<http://justpreprocessmyreads.sourceforge.net>) and were error corrected using Blue⁴⁶ with a ‘reference’
485 *kmer* dataset derived from the most recently collected 2x250 Illumina RNA-seq data and a coverage cut-off of
486 2. The Illumina RNA-Seq data was assembled using Trinity RNA-Seq version 2.1.1⁵⁸ with both the ‘*de-*
487 *novo*’ and ‘*genome-guided*’ options. The 454 data alongside all mRNA data acquired from GenBank and

488 public Illumina data acquired from NCBI SRA were assembled and clustered using MIRA 4.9.5⁵⁹. The
489 Trinity *de-novo*, Trinity *genome-guided* and the MIRA assemblies were aligned and assembled against the
490 genome using a new version of PASA (Haas et al. 2003; Haas, Papanicolaou *et al.* in preparation), thus,
491 creating a non-redundant, intron-aware transcript set referred here as PASA cDNA contigs. The new
492 Illumina RNA-Seq were aligned against the reference *H. erato* genome using GSNAP v.2015-09-29⁶¹
493 providing high-quality information of intron coordinates. Repetitive content was identified (simple,
494 complex/ transposable, *de-novo*, tRNA and rRNA elements) using trf⁶², RepeatModeler⁶³, RepeatScout⁶⁴,
495 RepeatMasker⁶³, RepBase data⁶⁵, tRNAScan⁶⁶ and Aragorn⁶⁷. This masked dataset was provided at the last
496 stage of the pipeline only.

497 We used two *de novo* gene modelers, GeneMark-ET⁶⁸ and Augustus 3.2.1⁶⁹ for gene prediction. Both used
498 the intron co-ordinates as external evidence. In addition, Augustus used further external evidence as hints
499 including the RNA-seq coverage derived from the Illumina reads, protein domains acquired from searching
500 the genome against Swissprot using the HHBlits program⁷⁰, a high-quality subset of the PASA cDNA
501 contigs as determined by JAMg, alignments of Uniref50 and the *Heliconius melpomene* predicted protein
502 set⁷¹. The Augustus HMM models were trained and evaluated using a ‘training’ and ‘test’ subsets of the
503 high-quality PASA cDNA contigs. Following this, the external evidence was weighted using the JAMg
504 optimization method and the same training and test cDNA contig datasets. At this point, we determined that
505 the repeatmasking data provided inferior prediction results and were not used in the final prediction. Finally,
506 Augustus was run with UTR prediction enabled to reduce false positive exons. Resulting UTRs were
507 removed from the final prediction.

508 The Repeat masking information, GenMark-ET, Augustus, PASA cDNA contigs, the Uniref50 and *H.*
509 *melpomene* protein alignments were provided to EvidenceModeler⁷² to derive a consensus gene dataset. This
510 consensus dataset was then twice edited with PASA2 in order to add alternative splicing information and
511 the UTRs as supported by cDNA evidence. This formed our Official Gene Set (OGS1). The OGS1 proteins
512 were then functionally annotated using Just_Annotate_My_Proteins (JAMp;
513 <https://github.com/genomecuration/JAMp>) searched against Hidden Markov Profiles of known proteins
514 with manually curated metadata (Swissprot; clustered at 70% identity and aligned). For each significant hit
515 (using the default settings of JAMp such as an e-value of 1e-10 and p-value of 1e-12), any Gene Ontology,
516 ENZYME and KEGG ontology terms of the known Swissprot proteins were linked to the *H. erato* predicted
517 proteins but only if the annotation evidence was experimentally derived and not inferred (i.e. terms with the
518 evidence codes of 'IEA', 'ISS', 'IEP', 'NAS', 'ND', 'NR' were ignored). The RNA-Seq data was finally aligned
519 against the OGS1 CDS data and processed with DEW (<https://github.com/alpapan/DEW>) to infer the
520 expression profiles for each gene. The functional and expression annotations are available from
521 http://annotation.insectacentral.org/heliconius_erato.

522
523 **Sequence alignment and variant calling:** We collected and sequenced 101 individual *H. erato* butterflies
524 from Peru (n = 15), French Guiana (n = 14), Suriname (n = 5), Ecuador (n = 29), Colombia (n = 12), Bolivia
525 (n = 4), Mexico (n = 6) and Panama (n = 16). We collected phenotypically pure (i.e. phenotypes resembling
526 the geographical *H. erato* races) individuals of each color pattern race from admixed populations where the
527 ranges of two color pattern races overlap. Additionally, we collected individuals from 8 different closely
528 related species including *H. ricini*, *H. sara*, *H. charithonia*, *H. hecalesia*, *H. telesiphe*, *H. hortense*, *H.*
529 *clysonimus*, and *H. hermathena* (Figure 1; Table S10,11 in SI section 4.1).

530 Whole genome 100 bp paired-end Illumina resequencing data of these individuals was aligned to the *H.*
531 *erato* v1 reference genome using BWA v0.7.13⁷³ with default parameters. PCR duplicated reads were
532 removed using Picard v1.138 (<http://picard.sourceforge.net>) and sorted using SAMtools⁷⁴. Genotypes were
533 called using the Genome Analysis Tool Kit (GATK) Haplotypecaller⁷⁵ with default parameters. Individual
534 genomic VCF records (gVCF) were jointly genotyped using GATK's genotypeGVCFs with default
535 parameters, except for setting expected heterozygosity to 0.025 to match the populations high heterozygosity
536 and grouping individuals according to race and sampling location. Genotype calls were only considered in
537 downstream analysis if they met the following criteria: Quality (QUAL) ≥ 30 , minimum depth ≥ 10 ,
538 maximum depth ≤ 100 (to avoid false SNPs due to mapping in repetitive regions), overall depth \leq
539 $100 \times$ number of samples, strand bias (FS) < 200 , Quality by depth ≥ 5 , and for variant calls, genotype quality
540 (GQ) ≥ 30 .

541
542 **Divergence and association analysis:** We estimated levels of relative (F_{ST})⁷⁶ and absolute genetic
543 divergence (d_{XY})⁷⁷, and nucleotide diversity (π)⁷⁷ between populations in sliding windows using python
544 scripts and egglib⁷⁸. In all our analyses, we only considered windows for which at least 10% of the positions
545 were genotyped for at least 75% of the individuals within each population. For the whole genome analysis
546 of the seven hybrid zones, on average 96.4% (SD = 1.1%) of windows met these criteria. Genotype by
547 phenotype (G x P) associations were tested for each variant position using a two-tailed Fisher's exact test.
548 Positions were excluded if less than 75% of individuals were genotyped for each phenotype. The sliding
549 window approach and the identification of distinct blocks of associated SNPs provides a robust approach
550 for identifying genomic regions of interests in our study system⁷⁹.

551
552 **Phylogenetic analysis:** We used FastTree v2.1⁸⁰ to infer an approximately maximum-likelihood phylogeny
553 from the entire genome using the default parameters. In this analysis, we only used concatenated SNP data
554 from chromosome 4-9, 11-14, 16, 17 and 20, because these chromosomes did not show any genetic
555 divergence peaks in our population analysis. FastTree computes support values on nodes using the

556 Shimodaira–Hasegawa test. Phylogenetic relationships of individuals across defined color pattern intervals
557 were constructed using Maximum Likelihood (ML) trees with RAxML v8.0.26⁸¹. The best likelihood tree
558 was chosen from 100 trees generated from a distinct starting tree using a GTR model with CAT
559 approximation of rate heterogeneity and the support values of this tree was inferred with 100 bootstrap
560 replicates.

561

562 **Phylogenetic weighting:** We applied a phylogenetic strategy for identifying shared or conserved genomic
563 intervals akin to ‘phylogenetic shadowing’⁸². We evaluated the support for alternative phylogenetic
564 hypotheses in the regions of peaks of divergence around color pattern loci using a novel method called
565 Topology Weighting by Iterative Sampling of Subtrees (*Twisst*: <https://github.com/simonhmartin/twisst>)²⁸.
566 This method solves the problem of describing the relationships between groups that are not necessarily
567 monophyletic. Given a tree and a set of pre-defined groups (in this case races) *Twisst* determines a weighting
568 for each possible topology describing the relationship of the groups (e.g. 6 groups yield 105 possible
569 unrooted topologies and therefore 105 weightings). Topology weightings are determined by sampling a
570 single member of each group and then identifying the topology matched by the resulting subtree. This
571 sampling is iterated over a large number of subtrees and weightings are calculated as the frequency of
572 occurrence of each topology. This method therefore reduces tree complexity caused by imperfect clustering
573 of samples within groups. The ability to consider all possible topologies at each window provides an
574 advantage over more commonly used likelihood ratio tests that only compare two topologies, which is
575 especially relevant for taxa that have potentially many distinct evolutionary histories across their genomes.
576 Weightings were estimated from 500 sampling iterations and averaged over ten bootstrap trees produced by
577 RAxML v8.0.26⁸¹ for each 2 kb window. Averaging weightings over bootstrap trees is expected to reduce
578 false support for certain phylogenetic groupings from trees with low bootstrap support.

579 For phylogenetic weighting along the *wntA* (chromosome 10) and *Ro* (chromosome 13) interval, we
580 compared weightings of topologies defined by samples from the following six groups: *H. e. demophoon*, *H.*
581 *e. etylus*, *H. e. notabilis*, *H. e. lativitta/emma*, *H. e. erato/amalfreda* and *H. e. hydara* (FG). To partly control
582 for the strong phylogeographic signal within *H. erato*, we focused these analyses on eastern Andean and
583 Amazonian races, which also show the most variation in forewing band shape, size and position. For the
584 *optix* (chromosome 18) interval, we compared weightings of topologies defined by samples from the
585 following six groups: *H. e. amalfreda*, *H. e. favorinus/hydara* (FG), *H. e. etylus/lativitta/emma/erato*, *H.*
586 *himera*, *H. telesiphe* and *H. clysonymus/hortense/hecalesia*. To obtain weightings for hypothesized
587 phylogenetic groupings of specific color pattern forms, we summed the counts of all topologies that were
588 consistent with the hypothesized grouping.

589

590 **Genotype weighting *optix*:** We evaluated genotypic similarity of species/races to the reference “postman”
591 haplotype using a sliding window analysis. The “postman” haplotype was defined based on the consensus
592 of fixed SNPs between all ‘postman’ (*H. e. demophoon*, *H. e. hydara* (Panama), *H. hydara* (French Guiana),
593 *H. e. notabilis* and *H. e. favorinus*) and all ‘rayed’ (*H. e. erato*, *H. e. etylus*, *H. e. emma* and *H. e. lativitta*)
594 *H. erato* races. In total there were 264 fixed SNPs across a 69 kb window on chromosome 18 near *optix*.
595 For each species/race evaluated, the proportion of SNPs that were identical to the postman haplotype was
596 calculated over windows of ten fixed SNPs, with a minimum coverage of 3 SNPs called in all individuals.
597 The window size and minimum coverage was chosen to best capture the turn-over of the genotypic similarity
598 along the genomic interval.

599
600 **Defining boundaries of color pattern intervals:** Our argument for identifying regulatory modules was
601 hierarchical. The association peaks, or regions of the genome containing clusters of sites perfectly associated
602 with wing pattern phenotype, marked the genomic intervals that likely contained the functional variation
603 responsible for phenotypic differences. We further resolved these intervals combining data across
604 independent transition zones. The rationale is that independent recombination events in the distinct locations
605 break down the pattern of associations, except at those very narrow intervals responsible for pattern
606 differences. Thus, in these areas individuals should group by color pattern phenotype rather than geographic
607 proximity, which is the pattern evident across the bulk of the genome. This is the basis of the *Twisst* analyses
608 described above. Specific boundaries are defined by a combination of *Twisst* and G X P association. For
609 example, near *wntA* and *optix*, we defined the boundary positions of the regulatory modules by overlaying
610 the phylogenetic weighting with genotype tables of the fixed allelic differences in the hybrid zone
611 comparisons. More precisely, at the regions where phylogenetic weighting support for phenotypic grouping
612 shifted and increased rapidly, we conservatively identified the boundaries of the intervals by looking for
613 patterns of shared genotypes between samples with similar phenotypes. It should be noted that this approach
614 assumes a single origin for functional alleles that are shared across similar phenotypes and will miss regions
615 where patterning alleles evolved independently. The boundaries of the regulatory modules near *Ro* and
616 *cortex* were defined only using the fixed SNP associations because the geographic distribution of the
617 phenotypes does not allow phylogenetic weighting to distinguish between geography and phenotypic
618 grouping for these loci.

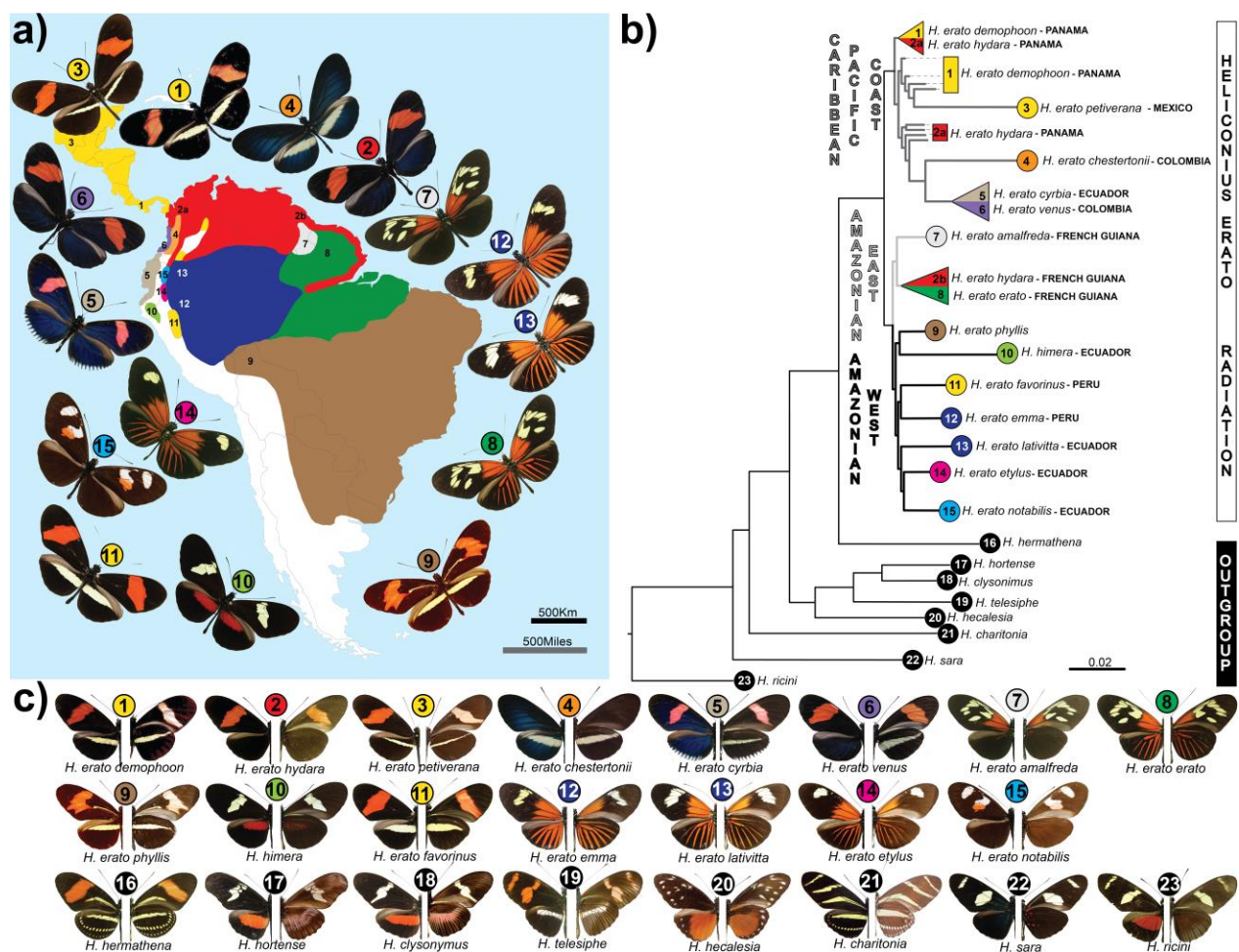
619

620

621 **Methods references**

- 622 45. Gnerre, S. *et al.* High-quality draft assemblies of mammalian genomes from massively parallel
623 sequence data. *Proc. Natl. Acad. Sci. U. S. A.* **108**, 1513–8 (2011).
- 624 46. Greenfield, P., Duesing, K., Papanicolaou, A. & Bauer, D. C. Sequence analysis Blue: correcting
625 sequencing errors using consensus and context. *Bioinformatics* **30**, 2723–2732 (2014).
- 626 47. Salmela, L. & Rivals, E. Sequence analysis LoRDEC: accurate and efficient long read error
627 correction. *Bioinformatics* **30**, 3506–3514 (2014).
- 628 48. Kurtz, S. *et al.* Versatile and open software for comparing large genomes. *Genome Biol.* **5**, R12
629 (2004).
- 630 49. English, A. C. *et al.* Mind the gap: upgrading genomes with Pacific Biosciences RS long-read
631 sequencing technology. *PLoS One* **7**, e47768 (2012).
- 632 50. Li, H. *et al.* The Sequence Alignment/Map format and SAMtools. *Bioinformatics* **25**, 2078–2079
633 (2009).
- 634 51. Rastas, P., Paulin, L., Hanski, I. & Lehtonen, R. Lep-MAP: fast and accurate linkage map
635 construction for large SNP datasets. *Bioinformatics* **29**, 3128–3134 (2013).
- 636 52. Rastas, P., Calboli, F. C. F., Guo, B., Shikano, T. & Merilä, J. Construction of ultradense linkage
637 maps with Lep-MAP2: Stickleback F2 recombinant crosses as an example. *Genome Biol. Evol.* **8**,
638 78–93 (2015).
- 639 53. Weisenfeld, N. I. *et al.* Comprehensive variation discovery in single human genomes. *Nat. Genet.*
640 **46**, 1350–1355 (2014).
- 641 54. Love, R. R., Weisenfeld, N. I., Jaffe, D. B., Besansky, N. J. & Neafsey, D. E. Evaluation of
642 DISCOVAR *de novo* using a mosquito sample for cost-effective short-read genome assembly.
643 *BMC Genomics* **17**, 187 (2016).
- 644 55. Li, H. Aligning sequence reads, clone sequences and assembly contigs with BWA-MEM. *arXiv*
645 1303.3997v1 (2013).
- 646 56. Smith, T. F. & Waterman, M. S. Identification of common molecular subsequences. *J. Mol. Biol.*
647 **147**, 195–197 (1981).
- 648 57. Simão, F. A., Waterhouse, R. M., Ioannidis, P. & Kriventseva, E. V. BUSCO: assessing genome
649 assembly and annotation completeness with single-copy orthologs. *Bioinformatics* **31**, 3210–3212
650 (2015).
- 651 58. Haas, B. J. *et al.* *De novo* transcript sequence reconstruction from RNA-seq using the Trinity
652 platform for reference generation and analysis. *Nat. Protoc.* **8**, 1494–512 (2013).
- 653 59. Chevreux, B. *et al.* Using the miraEST assembler for reliable and automated mRNA transcript
654 assembly and SNP detection in sequenced ESTs. *Genome Res.* **14**, 1147–1159 (2004).
- 655 60. Haas, B. J. *et al.* Improving the *Arabidopsis* genome annotation using maximal transcript alignment
656 assemblies. *Nucleic Acids Res.* **31**, 5654–5666 (2003).
- 657 61. Wu, T. D. & Nacu, S. Fast and SNP-tolerant detection of complex variants and splicing in short
658 reads. *Bioinformatics* **26**, 873–881 (2010).
- 659 62. Benson, G. Tandem repeats finder: a program to analyze DNA sequences. *Nucleic Acids Res.* **27**,
660 573–580 (1999).
- 661 63. Smit, A. F. A., Hubley, R. & Green, P. RepeatMasker. <http://www.repeatmasker.org/>. (2014).
- 662 64. Price, A. L., Jones, N. C. & Pevzner, P. a. *De novo* identification of repeat families in large
663 genomes. *Bioinformatics* **21**, i351–358 (2005).
- 664 65. Jurka, J. *et al.* Repbase Update, a database of eukaryotic repetitive elements. *Cytogenet. Genome*
665 *Res.* **110**, 462–467 (2005).
- 666 66. Lowe, T. M. & Eddy, S. R. tRNAscan-SE: a program for improved detection of transfer RNA
667 genes in genomic sequence. *Nucleic Acids Res.* **25**, 955–964 (1997).
- 668 67. Laslett, D. & Canback, B. ARAGORN, a program to detect tRNA genes and tmRNA genes in
669 nucleotide sequences. *Nucleic Acids Res.* **32**, 11–16 (2004).
- 670 68. Lomsadze, A., Burns, P. D. & Borodovsky, M. Integration of mapped RNA-Seq reads into

- 671 automatic training of eukaryotic gene finding algorithm. *Nucleic Acids Res.* **42**, e119 (2014).
- 672 69. Stanke, M., Schöffmann, O., Morgenstern, B. & Waack, S. Gene prediction in eukaryotes with a
673 generalized hidden Markov model that uses hints from external sources. *BMC Bioinformatics* **11**,
674 1–11 (2006).
- 675 70. Remmert, M., Biegert, A., Hauser, A. & Johannes, S. HHblits : Lightning-fast iterative protein
676 sequence searching by HMM-HMM alignment. *Nat. Methods* **9**, 173–175 (2012).
- 677 71. Davey, J. W. *et al.* Major improvements to the *Heliconius melpomene* genome assembly used to
678 confirm 10 chromosome fusion events in 6 million years of butterfly evolution. *G3* **6**, 695–708
679 (2016).
- 680 72. Haas, B. J. *et al.* Automated eukaryotic gene structure annotation using EVIDENCEModeler and the
681 Program to Assemble Spliced Alignments. *Genome Biol.* **9**, R7 (2008).
- 682 73. Li, H. & Durbin, R. Fast and accurate long-read alignment with Burrows-Wheeler transform.
683 *Bioinformatics* **26**, 589–595 (2010).
- 684 74. Li, H. *et al.* The Sequence Alignment / Map (SAM) Format and SAMtools 1000 Genome Project
685 Data Processing Subgroup. *Bioinformatics* **25**, 2078–2079 (2009).
- 686 75. Van der Auwera, G. a. *et al.* From fastQ data to high-confidence variant calls: The genome analysis
687 toolkit best practices pipeline. *Curr. Protoc. Bioinforma.* **UNIT 11.10**, 1–33 (2013).
- 688 76. Hudson, R. R., Slatkin, M. & Maddison, W. P. Estimation of levels of gene flow from DNA
689 sequence data. *Genetics* **132**, 583–589 (1992).
- 690 77. Nei, M. & Jin, L. Variances of the average numbers of nucleotide substitutions within and between
691 populations. *Mol. Biol. Evol.* **6**, 290–300 (1989).
- 692 78. De Mita, S. & Siol, M. EggLib: processing, analysis and simulation tools for population genetics
693 and genomics. *BMC Genet.* **13**, 27 (2012).
- 694 79. Nadeau, N. J. *et al.* Genomic islands of divergence in hybridizing *Heliconius* butterflies identified
695 by large-scale targeted sequencing. *Philos. Trans. R. Soc. Lond. B. Biol. Sci.* **367**, 343–353 (2012).
- 696 80. Price, M. N., Dehal, P. S. & Arkin, A. P. FastTree 2 – Approximately maximum-likelihood trees
697 for large alignments. *PLoS One* **5**, e9490 (2010).
- 698 81. Stamatakis, A. RAxML version 8: A tool for phylogenetic analysis and post-analysis of large
699 phylogenies. *Bioinformatics* **30**, 1312–1313 (2014).
- 700 82. Bofelli, D. *et al.* Phylogenetic shadowing of primate sequences to find functional regions of the
701 human genome. *Science* **299**, 1391–1394 (2003).
- 702



704

705

706

707

708

709

710

711

712

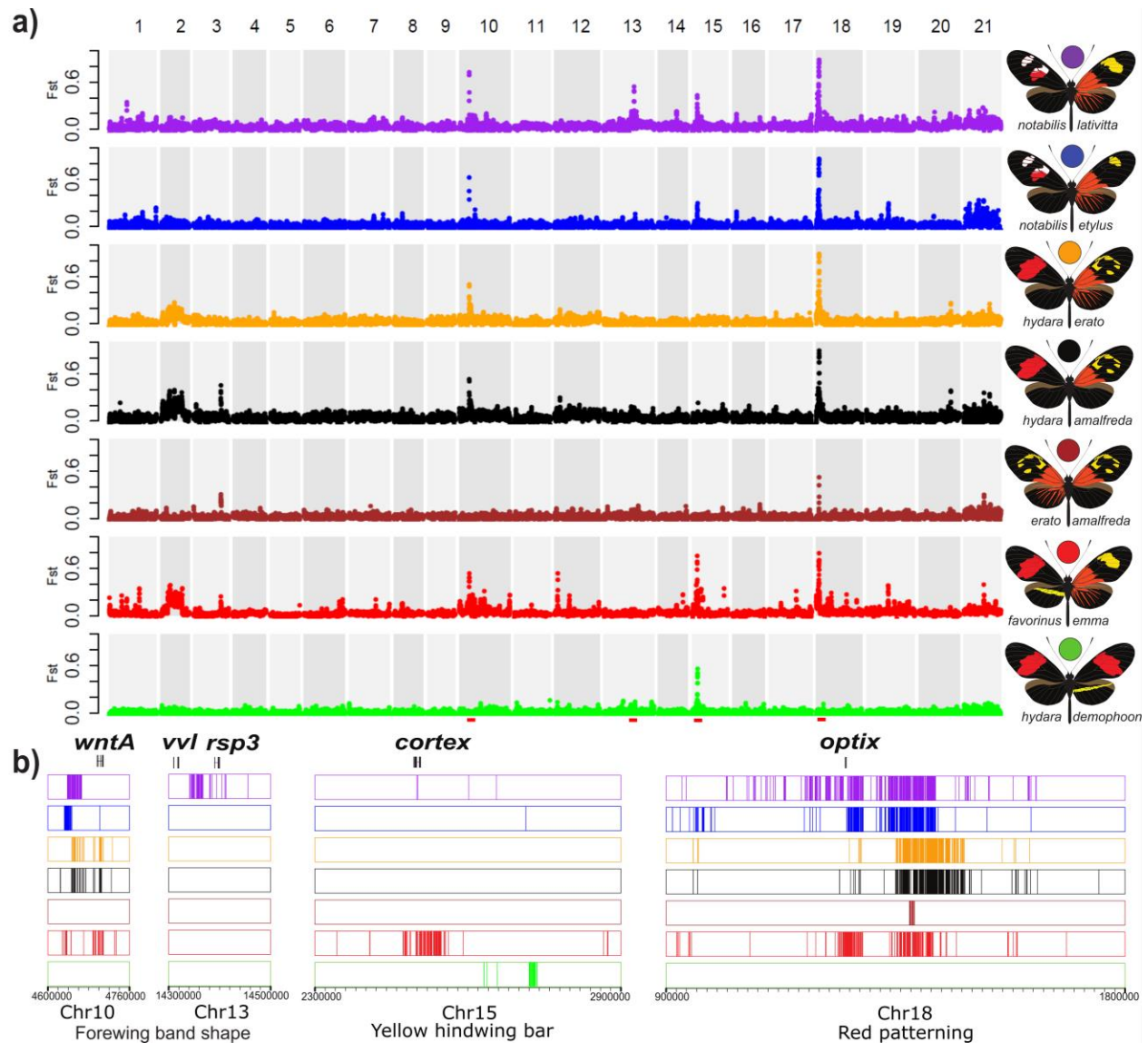
713

714

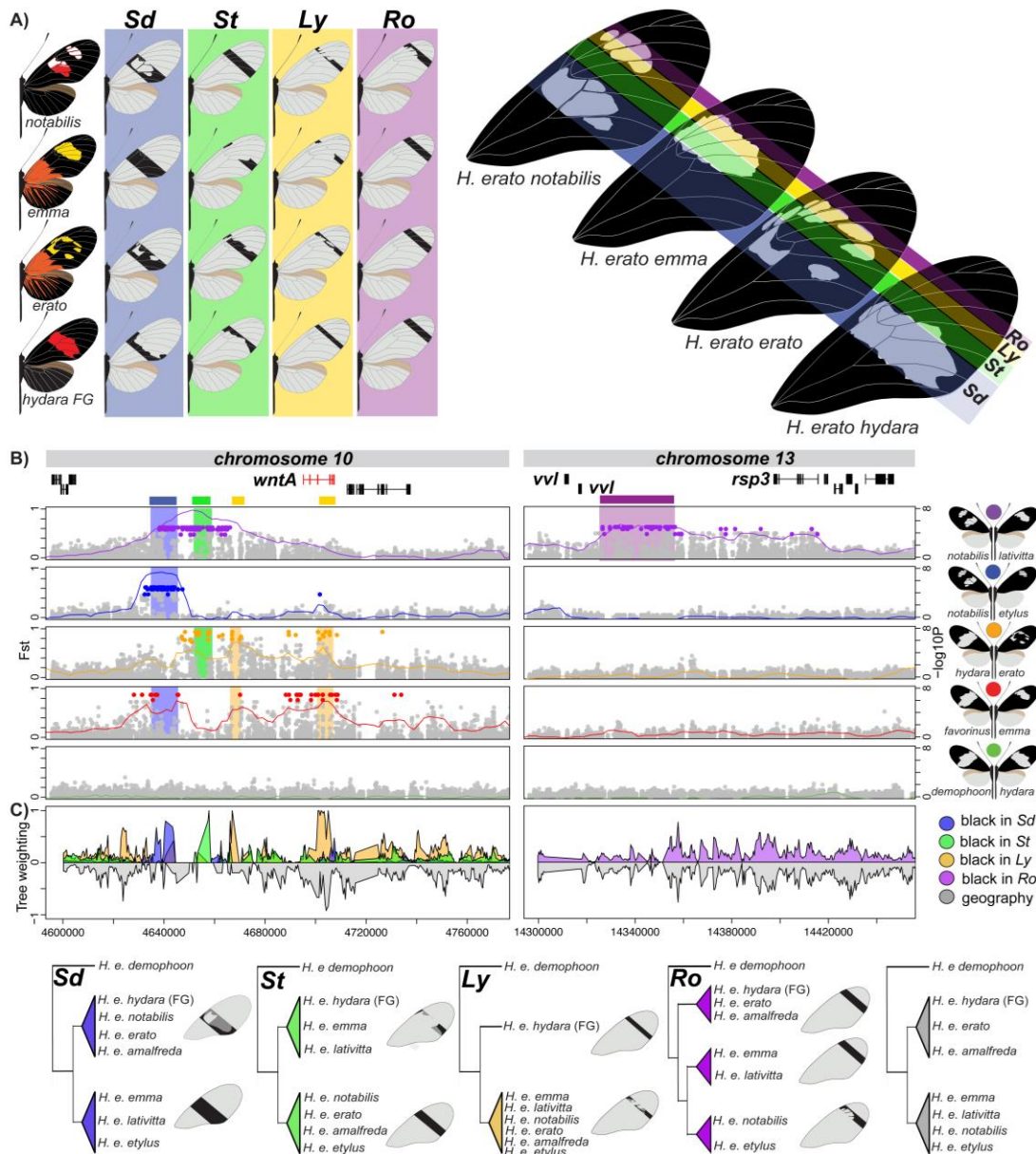
715

716

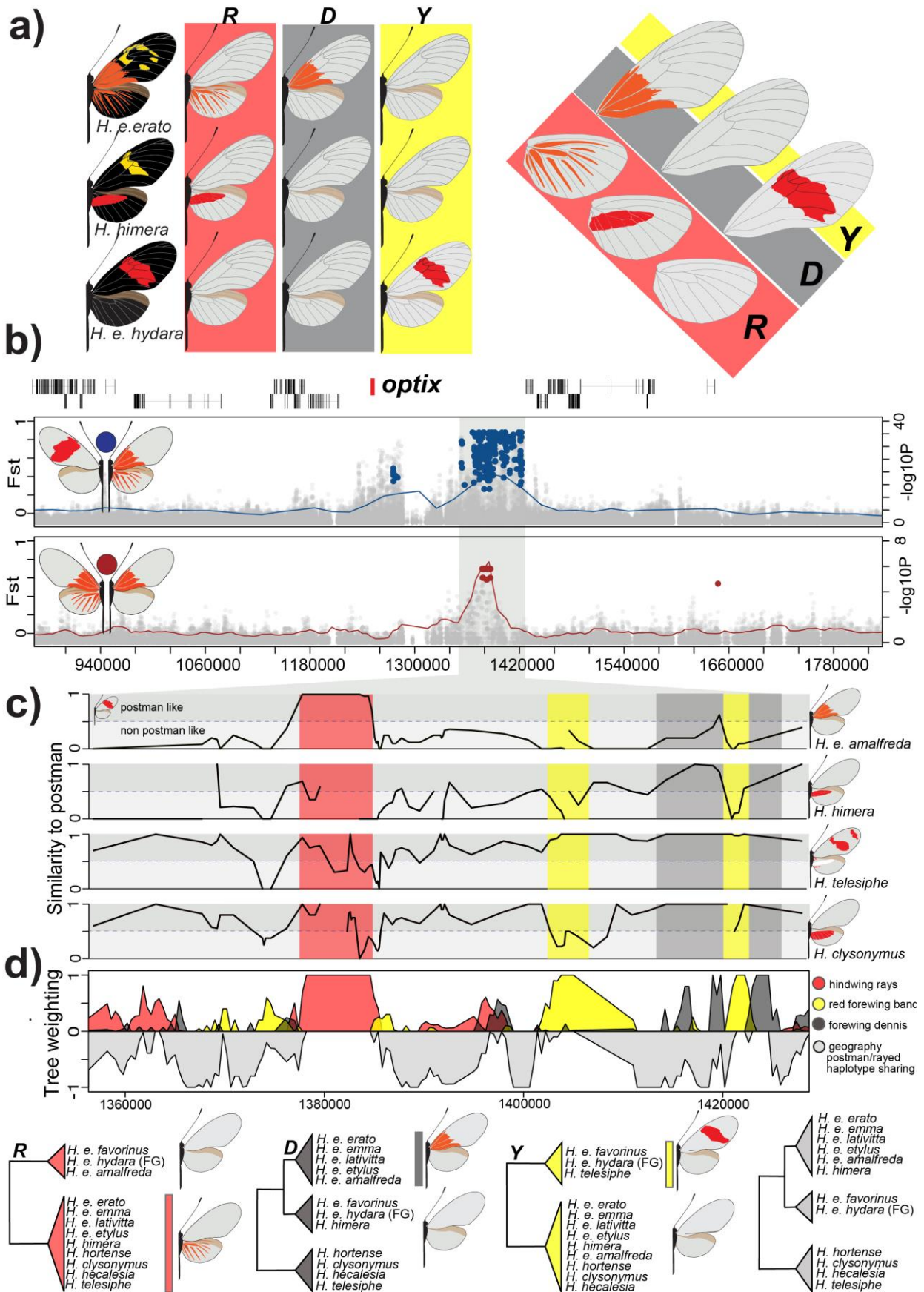
Figure 1. Geographical distribution, phylogeny and color pattern diversity of the *Heliconius erato* adaptive radiation. (a.) Geographical origin of samples; colors represent the distribution of the races; numbers are placed according to the sampling sites. (b.) Maximum likelihood tree based on autosomal sites located on chromosomes that do not show any marked F_{ST} peaks. All nodes shown had full local support based on the Shimodaira-Hasegawa test. Color and numbers represent, respectively, the geographical distribution and sampling site. On average five individuals were sequenced for each race and two for each outgroup species. All samples used in this study were included in the tree. There were three cases, (triangles) where individuals did not cluster together by racial designation (see Figure S5 for the full genome tree). (c.) Pictures of dorsal (left) and ventral (right) sides of the wings of races and species used in this study. Bottom row with black circles represent species that belong to the *erato* clade, but not to the *H. erato* adaptive radiation.



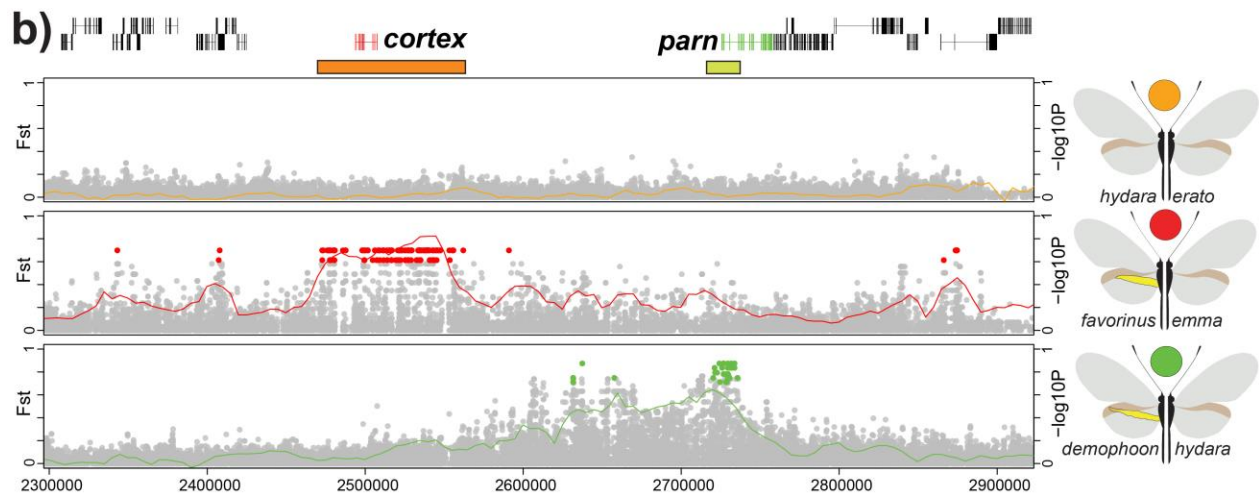
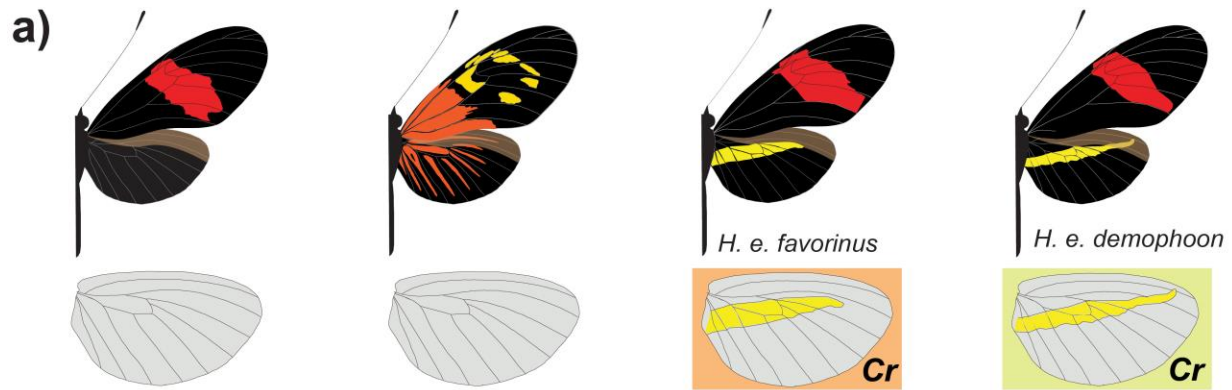
717
718
719 **Figure 2. Genomic divergence across the *Heliconius erato* phenotypic transition zones.** (a.) F_{ST} values were
720 calculated between color morphs from each of seven hybrid zones (indicated at right) and averaged over 50 kb windows
721 sliding in increments of 20 kb. Peaks represent regions of the genome with strongly divergent allele frequencies.
722 Divergence at chromosome 10, 15 and 18 corresponds with, respectively, divergence near the color pattern genes *wntA*,
723 *cortex* and *optix* (red dashes). These loci drive black forewing, yellow hindwing bar and red pigmentation patterns,
724 respectively. Importantly, between hybridizing races that were divergently colored, the only regions of the genome in
725 which we found fixed allelic differences were at the color pattern loci (see SI section 4.3 for a discussion of other
726 regions of the genome with increased divergence). (b.) Distribution of genotypes fixed between hybridizing races
727 located in the peaks of high divergence. This analysis revealed that, depending on the variable phenotype in the hybrid
728 zone, clusters of fixed SNPs are found in different genomic intervals near color pattern genes.
729



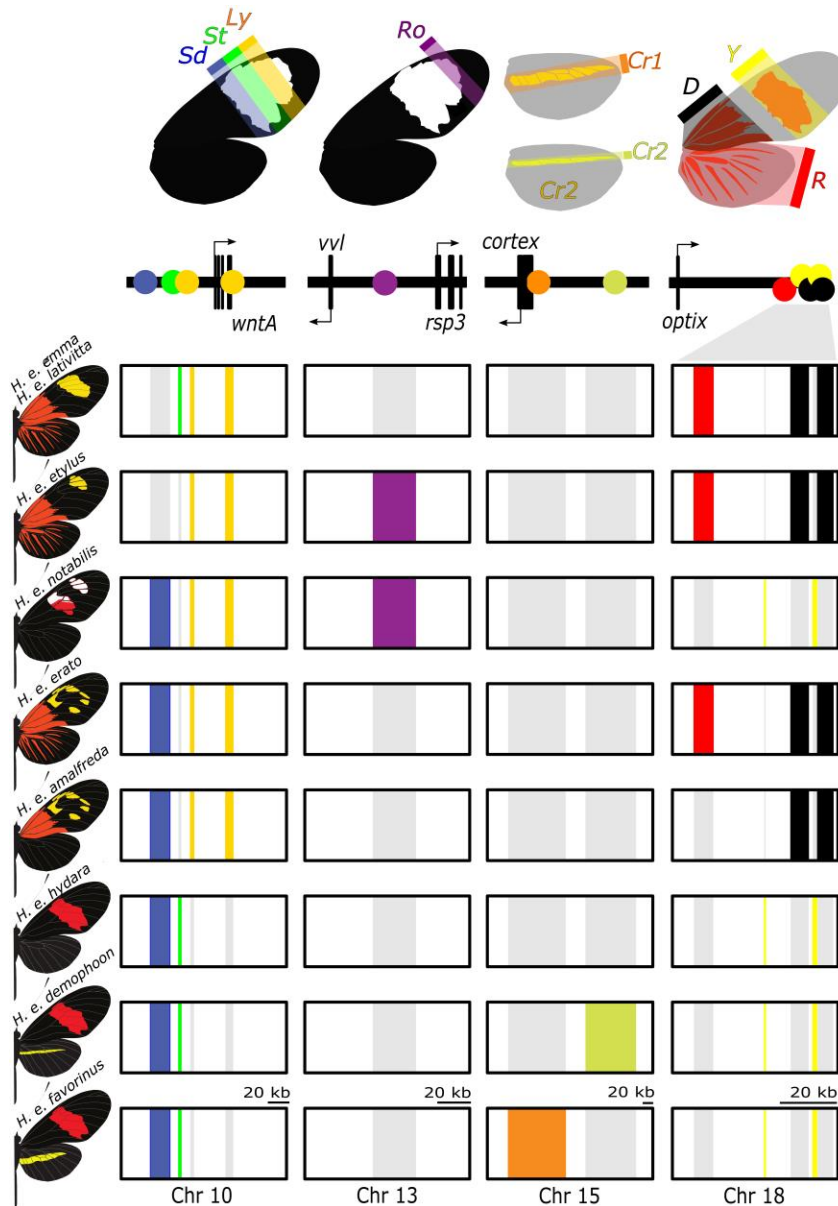
730
 731 **Figure 3. Association mapping in hybrid zones and phylogenetic comparisons identify the modular genetic**
 732 **architecture of black forewing variation.** (a.) Variation in black forewing patterning in the *H. erato* races. Black
 733 shading in the forewings highlights variation in melanin production in different parts of the forewing. Color shading
 734 corresponds to shading in panel B and C. (b.) F_{ST} (lines; 20 kb window, 5 kb step size) and association (points) analysis
 735 at the peaks of divergence in chromosome 10 and 13. Colored points represent associations estimated from fixed SNPs.
 736 (c.) Phylogenetic weighting of phenotypic hypothesis consistent with the *Sd*, *St*, *Ly* and *Ro* elements. These weightings
 737 were obtained by summing weightings for topologies that were consistent with the hypothesized groupings presented
 738 in the phylogenies. Tree topologies consistent with a geographic grouping are represented negative in gray. Within the
 739 genomic regions with high phylogenetic weighting support for a particular phenotypic hypothesis, we defined the
 740 boundaries of the color pattern intervals as position 4,634,972-4,641,535 for *Sd*, 4,657,452-4,658,207 for *St*, 4,666,909-
 741 4,670,474 for *Ly*₁ and 4,700,932-4,708,441 for *Ly*₂ on chromosome 10 and Position 14,341,251- 14,412,364 for *Ro* on
 742 chromosome 13. It is possible to further subdivided the *Sd* interval into two narrow intervals based on the phylogenetic
 743 weighting support and patterns of shared genotypes (position 4,637,657-4,637,727 for *Sd*₁, 4,639,853-4,641,535 for
 744 *Sd*₂). See SI, section 4.1.2 and 4.2.2 for the full phylogenetic trees of the identified intervals including all *H. erato*
 745 samples and closely related outgroup species.



747 **Figure 4. Modular architecture of red pattern variation.** (A.) Variation in red color patterning in the *H. erato* races
748 in the *ray* (*R*), *band* (*Y*) and *dennis* (*D*) region of the wings. (B.) F_{ST} (lines; 20 kb window, 5 kb step size) and association
749 (points) analysis at the peaks of divergence in the *optix* genomic region on chromosome 18 between races with red
750 rays and dennis patch (ray-dennis) versus races with a red forewing band (postman) (red; top panel) and *H. e. amalfreda*
751 (no rays) versus *H. e. erato* (rays) (brown; bottom panel). Colored points represent associations estimated from fixed
752 SNPs. (C.) Genotype weightings (10 SNP window, 5 SNP step size, 3 SNPs minimum genotyped in 50% of population)
753 of the positions that were identified as fixed between ray-dennis versus postman. A weighting of 1, means races or
754 species have the same genotypes as the postman races, whereas a weighting of 0 indicates completely different
755 genotypes in the considered window of fixed SNPs. (D.) Phylogenetic weighting of phenotypic hypothesis consistent
756 with the *R*, *Y* and *D* elements. These weightings were obtained by summing weightings for topologies that were
757 consistent with the hypothesized groupings presented in the phylogenies. Due to haplotype sharing among
758 Rayed/Dennis and Postman races, tree topologies consistent with geography are never supported in this genomic
759 interval. Support for topologies consistent with a geographic tree that accounts for this haplotype sharing are
760 represented upside-down in gray. We outlined the following positions: 1,377,801- 1,384,841 for *R*, 1,403,328-
761 1,412,865 for *Y*₁, 1,420,912-1,422,355 for *Y*₂, 1,412,888-1,419,375 for *D*₁ and 1,422,585-1,428,307 for *D*₂ on
762 chromosome 18. See SI, section 3.3.2 for the full phylogenetic trees of the identified intervals including all *H. erato*
763 samples and closely related outgroup species.
764



765
 766
 767 **Figure 5. Independent modules generate convergent yellow hindwing bar phenotypes** (a.) Variation in yellow
 768 hindwing bar in *H. e. favorinus* from Peru and *H. e. demophoon* from Panama. We note that the yellow hindwing bar
 769 morphology is not completely identical between these two races. While the yellow hindwing bar of *H. e. demophoon*
 770 is narrow, long and pointing up, *H. e. favorinus* exhibits a broader, shorter bar that points down. Shading corresponds
 771 to shading in panel b where two independent association peaks are identified. (b.) F_{ST} (lines; 20 kb window, 5 kb step
 772 size) and association (points) analysis near the *cortex* gene on chromosome 15. Comparison between *H. e. favorinus*
 773 and *H. e. emma* (red) shows a block of divergence different from the comparison between *H. e. demophoon* and *H. e.*
 774 *hydara* (green). The block of association between *H. e. demophoon* and *H. e. hydara* overlaps with the *parn* gene, but
 775 no functional link with color pattern variation has been identified for this gene¹⁶. Colored points represent associations
 776 estimated from fixed SNPs. Based on fixed SNP associations, we defined the positions of these two intervals as
 777 2,053,037-2,171,230 for *Cr*₁ (orange) and 2,211,881-2,315,926 for *Cr*₂ (yellow). See SI, section 4.4.2 for the full
 778 phylogenetic trees of the identified intervals including all *H. erato* samples and closely related outgroup species.
 779



780
 781
 782 **Figure 6. Modular regulatory architecture characterizes color pattern diversity within the *Heliconius erato***
 783 **radiation.** The upper panel provides a summary of color pattern variation found among *H. erato* butterflies that is
 784 related to spatial expression of the genes *wntA* (black forewing patterning; chromosome 10), *cortex* (yellow hindwing
 785 bar; chromosome 15), *optix* (red; chromosome 18) and a functionally uncharacterized genomic interval on chromosome
 786 13 responsible for pattern variation in the most distal region of the forewing band (*Ro*; functional candidates *vvl* and
 787 *rsp3*). The boxes in the bottom panel represent chromosomal intervals that include regulatory modules. These
 788 regulatory modules are colored for butterflies in which the pattern is expressed. The regulatory modules have been
 789 rearranged among *H. erato* races to generate distinct wing phenotypes. Note that for *Cr1* and *Cr2* and *rays* (*R*), band
 790 (*Y*) and *dennis* (*D*) patterns are expressed when, respectively, *cortex* and *optix* are expressed, whereas for *Sd*, *St* and *Ly*
 791 pattern expression corresponds with absence of *wntA* expression.